*aerospace*

MDPI

*Article*

# Refined Aircraft Positioning Based on Stochastic Hybrid Estimation with Adaptive Square-Root Unscented Particle Filtering

**Yangyang Zhang [1], Zhenxing Gao [2,*], Kai Qi [3] and Jiawei Li [1]**

[1] College of Civil Aviation, Nanjing University of Aeronautics and Astronautics, Nanjing 210016, China; zhang_yy@nuaa.edu.cn (Y.Z.); 1nhgxc1@nuaa.edu.cn (J.L.)
[2] College of General Aviation and Flight, Nanjing University of Aeronautics and Astronautics, Nanjing 210016, China
[3] Department of Flight, Shandong Airlines, Jinan 250014, China; qik@sda.cn
* Correspondence: z.x.gao@nuaa.edu.cn; Tel.: +86-1536-504-9918

**Abstract:** The positioning of civil aviation aircraft relative to a geographic reference point on Earth in a Cartesian frame is significant to detect the deviations from the desired path, especially for high-altitude airports or special airports based on performance-based navigation (PBN). To obtain these critical deviations during aircraft approach and landing, it is fundamental to estimate the continuous flight variables and discrete flight modes simultaneously with enough accuracy. With the coordinate conversion between the North, East, and Down (NED) frame and the geographic coordinate system based on World Geodetic System 1984 (WGS-84) considered, this study proposed a non-linear stochastic hybrid estimation algorithm with adaptive square-root unscented particle filtering (ASR-UPF) to estimate the true path. The probabilities of mode transition, represented by the normal cumulative density function of continuous states, determine whether to proceed with mode transitions. In addition, the adaptive update characterized by tracking variable noise and the importance sampling distributions based on the results of square-root unscented Kalman filtering (SR-UKF), as a comparative study of continuous system filtering, were used. The experiments illustrated the ASR-UPF is able to reduce the state estimation error more effectively, and more promptly track the error caused by incorrect mode estimation with adaptability compared to the SR-UKF. A further test with real flight data indicates that the proposed method gives the refined estimation of position and azimuth in NED frame.

**Keywords:** hybrid estimation; adaptive square-root unscented particle filtering; importance sampling; adaptive update



**Citation:** Zhang, Y.; Gao, Z.; Qi, K.; Li, J. Refined Aircraft Positioning Based on Stochastic Hybrid Estimation with Adaptive Square-Root Unscented Particle Filtering. *Aerospace* **2024**, *11*, 413. https://doi.org/10.3390/aerospace11050413

Academic Editor: Gokhan Inalhan

Received: 22 March 2024
Revised: 14 May 2024
Accepted: 17 May 2024
Published: 20 May 2024



## 1. Introduction

The deviations from the desired path of a civil aviation aircraft are significant for accident analysis, such as collision with obstacles, which needs positioning of the aircraft relative to obstacles, especially for high-altitude airports or special airports based on performance-based navigation (PBN) [1] that are positioned using global positioning systems (GPSs) with waypoints. Meanwhile, its positioning error is smaller than the protection area of traditional instrument flight procedure, and there are many tall obstacles around the airport. Consequently, it is necessary to estimate the position and azimuth in the Cartesian frame. Unfortunately, the position and azimuth of an aircraft relative to a geographic reference point on Earth in a Cartesian frame are not recorded in flight data, which provides support for solving the problem of positioning estimation in a Cartesian frame. When the aircraft is a highly complex nonlinear dynamic system, the continuous motion of the aircraft can make transitions between flight modes. Correspondingly, different modes can also change the patterns of the aircraft's continuous motion, that is, variable

aerodynamic configuration. Meanwhile, the flight data inevitably have uncertain noise due to uncertain factors such as navigation error, sensor measurement error, and external disturbances [2], and when integrated with manual operations, this could cause stochastic transitions between flight modes [3]. Therefore, the model of single-continuous-flight dynamics cannot match the variable aerodynamic configuration caused by mode transition, and a hybrid dynamics model should be established for discrete state and continuous state estimation.

Hybrid dynamics modeling mainly appears in the study of hybrid systems with coupled discrete and continuous states [4]. The earliest hybrid systems modeling formalized the underlying behavior and manual operations of the system using formal method [5]. However, this method, which has poor universality, uses strict formal language to express discrete mode transition, which has no description of continuous behavior. The mixed logical dynamic model (MLDM) contains the logic of continuous motion within discrete state transition logic, describing the transition of discrete states as a linear inequality containing both discrete and continuous variables via Boolean algebra and determines the mode transition based on the true or false logical conditions [6,7]. Nevertheless, MLDM characterized by deterministic probabilities of discrete state transition cannot reflect the uncertainty of flight mode transition. The generalized fuzzy hidden Markov model (GFHMM), extending HMM to the fuzzy domain, obtains the mode transition of automatic flight systems by fuzzy inference with two parameters, transition fuzzy density, and emission fuzzy density, which can be obtained through parameter statistical analysis or clustering algorithms [8,9]. However, the GFHMM does not take into account the mode transition caused by manual operations, and it is essentially a method for continuous time series analysis and prediction.

To demonstrate the stochastic mode transition, interacting multiple model (IMM) and constrained IMM take into account the probability of constant mode transition [10–13], which is limited to stochastic hybrid systems with discrete mode transitions that are independent of the continuous state variation. The state-dependent transition hybrid estimation (SDTHE) algorithm explicitly calculates the mode transition probabilities that depend on the continuous states [14]. Compared with IMM, SDTHE is more suitable for state estimation for general stochastic hybrid systems. Scholars have used the SDTHE algorithm to infer the intentions of the automatic flight system and compare them with the pilot's operational intentions to identify abnormal human–machine interactions [15]. By constraining the continuous state, the constrained SDTHE algorithm was developed for the estimation of unmanned aerial vehicle trajectory with turning constraints [16].

In cooperation with state estimation algorithms, this system can carry out state estimation based on the stochastic hybrid dynamic model with coupled discrete and continuous states. The extended Kalman filter (EKF), unscented Kalman filter (UKF), and cubature Kalman filter (CKF) based on KF have limited improvement of estimation accuracy for nonlinear systems [17–19], while particle filter could effectively solve this problem using sequential Monte Carlo sampling with the appropriate number of particles [20,21]. However, the importance of sampling distribution commonly uses a particle filter, which is generally a prior distribution, instead of using the posterior probability distribution corrected by measurement data, which would cause issues of low efficiency and sensitivity to singular points and would not effectively utilize measurement data [22]. Meanwhile, taking the posterior probability distribution generated by the square root unscented Kalman filter (SR-UKF) [23] as the importance sampling distribution not only utilizes new measurement data but also maintains computational stability in the form of the square root of covariance. In addition, due to the uncertainty of noise during filtering, adaptive methods need to be adopted to update the noise, which could improve the estimation accuracy of flight data further [24].

Considering that the aircraft is a highly nonlinear system, whose modes are numerous and complex, there is generally a problem of dimension explosion. Even though some solutions for simplifying state equations and measurement equations via aircraft mode

abstraction have been put forward [14,25], it would induce oversimplification if only the motion of the center of mass in a Cartesian frame were considered. In other words, calculating the coordinates of an aircraft in the Cartesian frame directly instead of converting coordinates between geographic and Cartesian frame would lead to inaccurate position calculations, which further cause excessive estimation error.

To estimate the position and azimuth of civil aviation aircraft with coupled modes and continuous states is fundamental to flight safety analysis and accident investigation. Focusing on the hybrid estimation of a nonlinear stochastic hybrid system, this study contributes to developing a synthetic filtering system characterized by the adaptive square-root unscented particle filtering (ASR-UPF) algorithm and considering the coordinate transformation via the track projection between a Cartesian frame and a geographic frame based on the World Geodetic System 1984 (WGS-84) to ensure high accuracy of the hybrid model [26]. In a simulation study and experiments on real flight data, the stochastic nonlinear hybrid estimation with ASR-UPF is tested and discussed deeply in this study.

This paper is organized as follows. In Section 2, the methodology of synthetic filtering system integrated with ASR-UPF and track projection is described, which is employed in hybrid system modeling and its estimation algorithm. In Section 3, the proposed algorithm is demonstrated with two examples of simulation tests and experiments on real flight data. The discussion and conclusions are presented in Section 4 and Section 5, respectively.

## 2. Methodology

A synthetic filtering system integrated with ASR-UPF and track projection is developed to estimate the relative position and azimuth of an aircraft in a Cartesian frame or local inertial frame, whose orientation is North, East, and Down $(x_n, y_n, z_n)$ with the defined origin.

### *2.1. Adaptive Square-Root Unscented Particle Filtering*

For continuous states, the state equation at time $k-1$ and the measurement equation at time $k$ are defined as

$$\begin{cases} \mathbf{x}_k^q = f^q\left(\mathbf{x}_{k-1}^q\right) + \boldsymbol{\omega}_{k-1}^q \\ \mathbf{y}_k = h^q\left(\mathbf{x}_k^q\right) + \mathbf{r}_k^q \end{cases} \tag{1}$$

where $q \in \mathbf{M}$ is the mode and $\mathbf{M}$ is the set consisting of $N_m$ modes. $\boldsymbol{\omega}_{k-1}^q$, $\mathbf{r}_k^q$ represent mutually independent Gaussian white noise at time $k-1$ and $k$, respectively.

At time $k = 0$, we define the initial mode as $q_0$, of which the probability is $\alpha_{0,q_0}^+ = 1$. The distribution of the initial continuous state corresponds to $N\left(\hat{\mathbf{x}}_{0,q_0}^+, \mathbf{Q}_0^{q_0}\right)$, from which sample $N$ particles $\hat{\mathbf{x}}_{0,q_0}^{+,n_p}, n_p = 1, 2, 3, \cdots, N$, and $\mathbf{Q}_0^{q_0}$ is the initial system noise covariance matrix obtained from the statistical analysis of historical flight data. The weights and square root of the covariance matrices of each particle are obtained as

$$\begin{cases} \tilde{w}_0^{q_0,n_p} = \dfrac{1}{N} \\ \mathbf{S}_0^{q_0,n_p} = \sqrt{\mathbf{Q}_0^{q_0}} \end{cases} \tag{2}$$

For the filter of other modes, we define the probabilities, the mean, and the square root of the covariance matrices of the continuous states as

$$\begin{cases} \alpha_{0,q}^+ = 0 \\ \hat{\mathbf{x}}_{0,q}^+ = \mathbf{0} \\ \mathbf{S}_0^q = \mathbf{0} \\ q \in \mathbf{M}, q \neq q_0 \end{cases} \tag{3}$$

Thus, the sampled particles and their weights of other modes are

$$\begin{cases} \hat{\mathbf{x}}_{0,q}^{+,n_p} = \mathbf{0} \\ \mathbf{S}_0^{q,n_p} = \mathbf{0} \\ \tilde{w}_0^{q,n_p} = \dfrac{1}{N} \end{cases} \tag{4}$$

At time $k-1$, the posterior distribution of each particle in each filter is $N\left(\hat{\mathbf{x}}_{k-1,q_{k-1}}^{+,n_p}, \left(\mathbf{S}_{k-1}^{q_{k-1},n_p}\right)^T \mathbf{S}_{k-1}^{q_{k-1},n_p}\right)$. The posterior probability of each discrete mode is $\alpha_{k-1,q_{k-1}}^{+}$, and the probability of mode transitions is $\gamma_k^{q_{k-1}q_k}$.

As the algorithm basis of ASR-UPF, the SR-UKF is described in the Appendix A1. To improve estimation accuracy, the adaptive filtering scheme is proposed, in which the two noise covariance matrices $\mathbf{Q}_k^{q_k,n_p}$ and $\mathbf{R}_k^{q_k,n_p}$ of particle $n_p$ in mode $q_k$ (or the $q_{k_{th}}$ filter) are able to be updated according to the error statistics. Then, the measurement noise covariance matrix is adjusted based on the a priori estimation in Equation (4) as

$$\begin{aligned} \mathbf{R}_k^{q_k,n_p} &= (1-d_k)\mathbf{R}_{k-1}^{q_{k-1},n_p} + d_k[\tilde{\mathbf{y}}_k^{q_k0,n_p}\left(\tilde{\mathbf{y}}_k^{q_k0,n_p}\right)^T - \\ &\sum_{row=0}^{2n} W_{row}^{q_k0,n_p(c)}(\hat{\mathbf{y}}_k^{q_k0,n_p(row)-} - \hat{\mathbf{y}}_k^{q_k0,n_p-})(\hat{\mathbf{y}}_k^{q_k0,n_p(row)-} - \hat{\mathbf{y}}_k^{q_k0,n_p-})^T] \end{aligned} \tag{5}$$

where the weights $d_k \in [0,1]$ determine the window length in adaptive filtering. With equal weights, the estimation will gradually become accurate if the noise characteristics remain unchanged. However, the weights with exponential fading are more appropriate to deal with the variation in the noise characteristics:

$$d_k = (1-b)/(1-b^{k+1}) \tag{6}$$

where $b \in (0,1)$ is the forgetting factor. Therefore, the square root of the measurement noise covariance matrix is derived as

$$\begin{aligned} \sqrt{\mathbf{R}_k^{q_k,n_p}}^T \sqrt{\mathbf{R}_k^{q_k,n_p}} &= \left[\sqrt{(1-d_k)}(\sqrt{\mathbf{R}_{k-1}^{q_{k-1},n_p}})^T \quad \sqrt{d_k}\tilde{\mathbf{y}}_k^{q_k0,n_p}\right] \left[\begin{array}{c} \left(\sqrt{(1-d_k)}\sqrt{\mathbf{R}_{k-1}^{q_{k-1},n_p}}\right)^T \\ \sqrt{d_k}\tilde{\mathbf{y}}_k^{q_k0,n_p} \end{array}\right] \\ &- \sum_{row=1}^{2n} \sqrt{d_k W_{row}^{q_k0,n_p(c)}}(\hat{\mathbf{y}}_k^{q_k0,n_p(row)-} - \hat{\mathbf{y}}_k^{q_k0,n_p-}) \left[\sqrt{d_k W_{row}^{q_k0,n_p(c)}}(\hat{\mathbf{y}}_k^{q_k0,n_p(row)-} - \hat{\mathbf{y}}_k^{q_k0,n_p-})\right]^T \\ &- sgn(W_0^{q_k0,n_p(c)})\left(\sqrt{d_k\left|W_0^{q_k0,n_p(c)}\right|}\right)^2 (\hat{\mathbf{y}}_k^{q_k0,n_p(0)-} - \hat{\mathbf{y}}_k^{q_k0,n_p-})(\hat{\mathbf{y}}_k^{q_k0,n_p(0)-} - \hat{\mathbf{y}}_k^{q_k0,n_p-})^T \end{aligned} \tag{7}$$

In computer implementation, the QR decomposition is carried out to obtain $\mathbf{R}_k^{q_k,n_p}$, and the Cholesky factor of the rank-1 update is carried out twice as

$$\begin{cases} \sqrt{\mathbf{R}_k^{q_k,n_p}} = qr\left\{\left[\sqrt{(1-d_k)}\sqrt{\mathbf{R}_{k-1}^{q_{k-1},n_p}}, \sqrt{d_k}\left(\tilde{\mathbf{y}}_k^{q_k0,n_p}\right)^T\right]^T\right\} \\ \sqrt{\mathbf{R}_k^{q_k,n_p}} = cholupdate(\sqrt{\mathbf{R}_k^{q_k,n_p}}, \sqrt{d_k W_{1:2n}^{q_k0,n_p(c)}}\left(\hat{\mathbf{y}}_k^{q_k0,n_p(1:2n)-} - \hat{\mathbf{y}}_k^{q_k0,n_p-}\right),' -') \\ \sqrt{\mathbf{R}_k^{q_k,n_p}} = cholupdate(\sqrt{\mathbf{R}_k^{q_k,n_p}}, \sqrt{d_k\left|W_0^{q_k0,n_p(c)}\right|}\left(\hat{\mathbf{y}}_k^{q_k0,n_p(0)-} - \hat{\mathbf{y}}_k^{q_k0,n_p-}\right),' -(sgn(W_0^{q_k0,n_p(c)}))') \\ \sqrt{\mathbf{R}_k^{q_k,n_p}} = diag(diag(\sqrt{\mathbf{R}_k^{q_k,n_p}})) \end{cases} \tag{8}$$

where *diag* represents the diagonal matrix. After the adaptive update of $\mathbf{R}_k^{q_k,n_p}$, the measurement update is performed based on traditional SR-UKF, as shown in Equation (A5).

To complete the adaptation operation, the process noise covariance matrix $\mathbf{Q}_k^{q_k,n_p}$, updated based on the a priori estimation in Equation (A3) and a posteriori estimation in Equation (A6), is adjusted as follows:

$$\begin{aligned}\mathbf{Q}_k^{q_k,n_p} &= (1-d_k)\mathbf{Q}_{k-1}^{q_{k-1},n_p} \\ &+ d_k\left(\left(\hat{\mathbf{x}}_k^{q_k 0,n_p+} - \hat{\mathbf{x}}_k^{q_k 0,n_p-}\right)\left(\hat{\mathbf{x}}_k^{q_k 0,n_p+} - \hat{\mathbf{x}}_k^{q_k 0,n_p-}\right)^T - \mathbf{U}_k^{q_k,n_p}\left(\mathbf{U}_k^{q_k,n_p}\right)^T\right)\end{aligned} \tag{9}$$

After the QR decomposition and Cholesky factor of rank-1 update,

$$\begin{aligned}\sqrt{\mathbf{Q}_k^{q_k,n_p}}^T\sqrt{\mathbf{Q}_k^{q_k,n_p}} &= \begin{bmatrix}\sqrt{(1-d_k)}\sqrt{\mathbf{Q}_{k-1}^{q_{k-1},n_p}} \\ \sqrt{d_k}(\hat{\mathbf{x}}_k^{q_k 0,n_p+} - \hat{\mathbf{x}}_k^{q_k 0,n_p-})^T\end{bmatrix}^T\begin{bmatrix}\sqrt{(1-d_k)}\sqrt{\mathbf{Q}_{k-1}^{q_{k-1},n_p}} \\ (\sqrt{d_k}(\hat{\mathbf{x}}_k^{q_k 0,n_p+} - \hat{\mathbf{x}}_k^{q_k 0,n_p-}))^T\end{bmatrix} \\ &- \sqrt{d_k}\mathbf{U}_k^{q_k,n_p}(\sqrt{d_k}\mathbf{U}_k^{q_k,n_p})^T\end{aligned} \tag{10}$$

In computer implementation, the square root of the process noise covariance matrix is derived by

$$\begin{cases}\sqrt{\mathbf{Q}_k^{q_k,n_p}} = qr\left\{\left[\sqrt{(1-d_k)}\sqrt{\mathbf{Q}_{k-1}^{q_{k-1},n_p}}, (\sqrt{d_k}(\hat{\mathbf{x}}_k^{q_k 0,n_p+} - \hat{\mathbf{x}}_k^{q_k 0,n_p-}))^T\right]^T\right\} \\ \sqrt{\mathbf{Q}_k^{q_k,n_p}} = cholupdate(\sqrt{\mathbf{Q}_k^{q_k,n_p}}, \sqrt{d_k}\mathbf{U}_k^{q_k,n_p}, '-') \\ \sqrt{\mathbf{Q}_k^{q_k,n_p}} = diag(diag(\sqrt{\mathbf{Q}_k^{q_k,n_p}}))\end{cases} \tag{11}$$

Define $N\left(\hat{\mathbf{x}}_k^{q_k 0,n_p+}, \mathbf{S}_k^{q_k 0,n_p}\left(\mathbf{S}_k^{q_k 0,n_p}\right)^T\right)$ according to Equation (A6) as the importance sampling distribution, from which we obtain $\hat{\mathbf{x}}_{k,q_k}^{+,n_p}$ particles and calculate the weight of each particle. Then, the weight of each particle is updated and normalized as follows:

$$\begin{cases}w_k^{q_k,n_p} = \tilde{w}_{k-1}^{q_{k-1},n_p}\dfrac{N\left(\mathbf{y}_k; \hat{\mathbf{x}}_{k,q_k}^{+,n_p}, \sqrt{\mathbf{R}_k^{q_k,n_p}}\left(\sqrt{\mathbf{R}_k^{q_k,n_p}}\right)^T\right)}{N\left(\hat{\mathbf{x}}_{k,q_k}^{+,n_p}; \hat{\mathbf{x}}_k^{q_k 0,n_p+}, \mathbf{S}_k^{q_k 0,n_p}\left(\mathbf{S}_k^{q_k 0,n_p}\right)^T\right)} \\ * N\left(\hat{\mathbf{x}}_{k,q_k}^{+,n_p}; \hat{\mathbf{x}}_{k-1,q_{k-1}}^{+,n_p}, \sqrt{\mathbf{Q}_{k-1}^{q_{k-1},n_p}}\left(\sqrt{\mathbf{Q}_{k-1}^{q_{k-1},n_p}}\right)^T\right) \\ \tilde{w}_k^{q_k,n_p} = \dfrac{w_k^{q_k,n_p}}{\sum_{n_p=1}^N w_k^{q_k,n_p}}\end{cases} \tag{12}$$

We determine whether to perform resampling based on the number of valid particles and calculate the number of valid particles as follows [27]:

$$\hat{N}_{eff} = \frac{1}{\sum_{n_p=1}^N\left(w_k^{q_k,n_p}\right)^2} \tag{13}$$

If $\hat{N}_{eff} < N_{threshold}$, where $N_{threshold}$ represents the threshold of particle number, we perform random resampling and make $\tilde{w}_k^{q_k,n_p} = \frac{1}{N}$. The algorithm pseudocode is shown in Algorithm 1.

**Algorithm 1:** Adaptive Square-Root Unscented Particle Filter

At time $k = 0$: Sample $N$ particles from the prior distribution $p(x_0)$
**for** $k = 1, 2, 3, \ldots$ **do**
**Importance sampling**: Sample $N$ particles from the distribution $N\left(\hat{\mathbf{x}}_k^{q_k 0, n_p +}, \mathbf{S}_k^{q_k 0, n_p}\left(\mathbf{S}_k^{q_k 0, n_p}\right)^T\right)$ by the SR-UKF
**Resampling**: Update the weights with Equation (12) and determine whether to perform random resampling based on Equation (13)
**Adaptive update**: Update $\sqrt{\mathbf{Q}_k^{q_k, n_p}}$ and $\sqrt{\mathbf{R}_k^{q_k, n_p}}$ using Equations (11) and (8), respectively
**Output**: Update the estimation with Equation (20)
**end**

### 2.2. Stochastic Hybrid Estimation with ASR-UPF

As shown in Figure 1. For discrete states, the set of conditions for mode transition is

$$D^{St}(q_{k-1}, q_k) = \left\{ [\mathbf{x}_{k-1}, q_{k-1}, \boldsymbol{\zeta}]^T | (\mathbf{L}_{q_{k-1} q_k} [\mathbf{x}_{k-1}^T \boldsymbol{\zeta}^T]^T \leq 0 | q_{k-1}) \right\} \tag{14}$$

where $\mathbf{L}_{q_{k-1} q_k}$ is a constant matrix, and is $\boldsymbol{\zeta}$ the logic judgment variable of mode transition, which refers to the combination of continuous flight parameters that affect mode transition and could be obtained from historical flight data through data statistics. The posterior probability of mode $q_{k-1}$ is given as follows:

$$\alpha_{k-1, q_{k-1}}^{+} = p(q_{k-1} | \mathbf{Y}_{k-1}) \tag{15}$$

where $\mathbf{Y}_{k-1} = \{\mathbf{y}_1, \mathbf{y}_2, \cdots, \mathbf{y}_{k-1}\}$ represents the time series of measurements. $q_{k-1}$ represents the mode at time $k-1$.

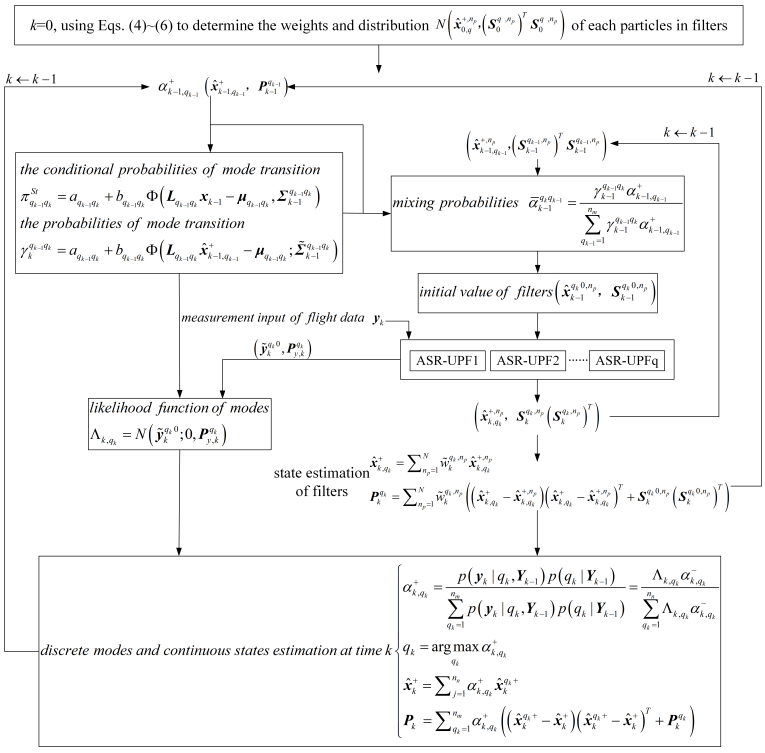


**Figure 1.** Structure of the nonlinear SHE algorithm.

Thus, the conditional posterior probability of a continuous state at time $k-1$ is $N\left(\boldsymbol{\mu}_{q_{k-1}q_k}, \boldsymbol{\Sigma}_{k-1}^{q_{k-1}q_k}\right)$. We define conditional mode transition probability as [15]:

$$\begin{aligned} \pi_{q_{k-1}q_k}^{St} &= p(q_k|q_{k-1}, \mathbf{x}_{k-1}) = p([\mathbf{x}_{k-1}, q_{k-1}, \boldsymbol{\zeta}]^T \in D^{St}(q_{k-1}, q_k)) \\ &= a_{q_{k-1}q_k} + b_{q_{k-1}q_k}\Phi\left(\mathbf{L}_{q_{k-1}q_k}\mathbf{x}_{k-1} - \boldsymbol{\zeta}_{q_{k-1}q_k}, \boldsymbol{\Sigma}_{k-1}^{q_{k-1}q_k}\right) \end{aligned} \tag{16}$$

where $\Phi(\cdot)$ represents the normal cumulative density function, and $\boldsymbol{\zeta}_{q_{k-1}q_k}$ is the judgment variable for mode transition logic, and its distribution can be obtained by statistical analysis of flight data (e.g., we obtain the continuous flight parameters related to mode transition of a certain aircraft model, and obtain the distribution of these parameters in a parametric test). $\boldsymbol{\Sigma}_{k-1}^{q_{k-1}q_k}$ is the constant matrix of $\boldsymbol{\zeta}_{q_{k-1}q_k}$. $a_{q_{k-1}q_k}, b_{q_{k-1}q_k}$ are scalar constants such that $\pi_{q_{k-1}q_k}^{St} \geq 0$ for all $q_{k-1}, q_k \in \mathbf{M}$, and $\sum_{q_k=1}^{N_m} \pi_{q_{k-1}q_k}^{St} = 1$.

Then, the probability of mode transition is derived as follows:

$$\begin{cases} \gamma_k^{q_{k-1}q_k} = p(q_k|q_{k-1}, \mathbf{Y}_{k-1}) = a_{q_{k-1}q_k} + b_{q_{k-1}q_k}\Phi\left(\mathbf{L}_{q_{k-1}q_k}\hat{\mathbf{x}}_{k-1,q_{k-1}}^{+} - \boldsymbol{\mu}_{q_{k-1}q_k}; \tilde{\boldsymbol{\Sigma}}_{k-1}^{q_{k-1}q_k}\right) \\ \tilde{\boldsymbol{\Sigma}}_{k-1}^{q_{k-1}q_k} = \boldsymbol{\Sigma}_{k-1}^{q_{k-1}q_k} + \mathbf{L}_{q_{k-1}q_k}\mathbf{P}_{k-1}^{q_{k-1}}\mathbf{L}_{q_{k-1}q_k} \end{cases} \tag{17}$$

where $\boldsymbol{\mu}_{q_{k-1}q_k}$ is the mean of $\boldsymbol{\imath}_{q_{k-1}q_k}$ and $\mathbf{P}_{k-1}^{q_{k-1}}$ is the covariance matrix of $\hat{\mathbf{x}}_{k-1,q_{k-1}}^{+}$, which can be obtained as follows:

$$\begin{cases} \hat{\mathbf{x}}_{k-1,q_{k-1}}^{+} = \sum\limits_{n_p=1}^{N} \tilde{w}_{k-1}^{q_{k-1},n_p}\hat{\mathbf{x}}_{k-1,q_{k-1}}^{+,n_p} \\ \tilde{\boldsymbol{\Sigma}}_{k-1}^{q_{k-1}q_k} = \boldsymbol{\Sigma}_{k-1}^{q_{k-1}q_k} + \mathbf{L}_{q_{k-1}q_k}\left(\mathbf{S}_{k-1}^{q_{k-1}}\right)^T\mathbf{S}_{k-1,}^{q_{k-1}}\mathbf{L}_{q_{k-1}q_k}^T \\ \mathbf{P}_{k-1}^{q_{k-1}} = \sum\limits_{n_p=1}^{N} \tilde{w}_{k-1}^{q_{k-1},n_p}\left(\hat{\mathbf{x}}_{k-1,q_{k-1}}^{+,n_p} - \hat{\mathbf{x}}_{k-1,q_{k-1}}^{+}\right)\left(\hat{\mathbf{x}}_{k-1,q_{k-1}}^{+,n_p} - \hat{\mathbf{x}}_{k-1,q_{k-1}}^{+}\right)^T \\ \quad + \sum\limits_{n_p=1}^{N} \tilde{w}_{k-1}^{q_{k-1},n_p}\left(\mathbf{S}_{k-1}^{q_{k-1},n_p}\right)^T\mathbf{S}_{k-1}^{q_{k-1},n_p} \\ \mathbf{S}_{k-1}^{q_{k-1}} = qr\left\{\left[\sum\limits_{n_p=1}^{N}\sqrt{\tilde{w}_{k-1}^{q_{k-1},n_p}}\left(\hat{\mathbf{x}}_{k-1,q_{k-1}}^{+,n_p} - \hat{\mathbf{x}}_{k-1,q_{k-1}}^{+}\right), \sum\limits_{n_p=1}^{N}\sqrt{\tilde{w}_{k-1}^{q_{k-1},n_p}}\left(\mathbf{S}_{k-1}^{q_{k-1},n_p}\right)\right]^T\right\} \end{cases} \tag{18}$$

Initial value of each filter can be obtained as follows:

$$\begin{cases} \hat{\mathbf{x}}_{k-1}^{q_k0,n_p} = \sum\limits_{q_{k-1}=1}^{n_m} \hat{\mathbf{x}}_{k-1,q_{k-1}}^{+,n_p}\bar{\alpha}_{k-1}^{q_kq_{k-1}} \\ \mathbf{P}_{k-1}^{q_k0,n_p} = \sum\limits_{q_{k-1}=1}^{n_m}\left(\left(\mathbf{S}_{k-1}^{q_{k-1},n_p}\right)^T\mathbf{S}_{k-1}^{q_{k-1},n_p} + \left(\hat{\mathbf{x}}_{k-1,q_{k-1}}^{+,n_p} - \hat{\mathbf{x}}_{k-1}^{q_k0,n_p}\right)\left(\hat{\mathbf{x}}_{k-1,q_{k-1}}^{+,n_p} - \hat{\mathbf{x}}_{k-1}^{q_k0,n_p}\right)^T\right)\bar{\alpha}_{k-1}^{q_kq_{k-1}} \\ \mathbf{S}_{k-1}^{q_k0,n_p} = qr\left\{\sqrt{\bar{\alpha}_{k-1}^{q_kq_{k-1}}}\left[\sum\limits_{q_{k-1}=1}^{n_m}\mathbf{S}_{k-1,\cdot|q_{k-1}}^{T}, \sum\limits_{q_{k-1}=1}^{n_m}\left(\hat{\mathbf{x}}_{k-1,\cdot|q_{k-1}}^{+} - \hat{\mathbf{x}}_{k-1}^{q_k0}\right)\right]^T\right\} \\ \bar{\alpha}_{k-1}^{q_kq_{k-1}} = p(q_{k-1}|q_k, \mathbf{Y}_{k-1}) = \dfrac{\gamma_{k-1}^{q_{k-1}q_k}\alpha_{k-1,q_{k-1}}^{+}}{\sum\limits_{q_{k-1}=1}^{n_m}\gamma_{k-1}^{q_{k-1}q_k}\alpha_{k-1,q_{k-1}}^{+}} \end{cases} \tag{19}$$

Further, we obtain the filtering values for each mode using the ASR-UPF filter based on Equation (19):

$$\begin{cases} \hat{\mathbf{x}}_k^{q_k+} = \sum_{n_p=1}^{N} \tilde{w}_k^{q_k,n_p} \hat{\mathbf{x}}_{k,q_k}^{+,n_p} \\ \mathbf{P}_k^{q_k} = \sum_{n_p=1}^{N} \tilde{w}_k^{q_k,n_p} \left( \left( \hat{\mathbf{x}}_k^{q_k+} - \hat{\mathbf{x}}_{k,q_k}^{+,n_p} \right) \left( \hat{\mathbf{x}}_k^{q_k+} - \hat{\mathbf{x}}_{k,q_k}^{+,n_p} \right)^T + \mathbf{S}_k^{q_k 0,n_p} \left( \mathbf{S}_k^{q_k 0,n_p} \right)^T \right) \end{cases} \tag{20}$$

Meanwhile, the residual and its covariance matrix can be obtained as follows:

$$\begin{cases} \tilde{\mathbf{y}}_k^{q_k 0} = \sum_{n_p=1}^{N} \tilde{w}_k^{q_k,n_p} \left( \mathbf{y}_k - \hat{\mathbf{y}}_k^{q_k 0,n_p -} \right) \\ \mathbf{P}_{y,k}^{q_k} = \sum_{n_p=1}^{N} \tilde{w}_k^{q_k,n_p} \mathbf{S}_{y,k}^{q_k,n_p} \left( \mathbf{S}_{y,k}^{q_k,n_p} \right)^T \end{cases} \tag{21}$$

The mode prior probability is derived as follows:

$$\alpha_{k,q_k}^{-} = p(q_k|\mathbf{Y}_k) = \sum_{q_{k-1}=1}^{n_m} \gamma_{k-1}^{q_{k-1},q_k} \alpha_{k-1,q_{k-1}}^{+} \tag{22}$$

We define likelihood function of the $q_{k_{th}}$ filter as follows:

$$\Lambda_{k,q_k} = p(\mathbf{y}_k|q_k, \mathbf{Y}_{k-1}) = N\left( \tilde{\mathbf{y}}_k^{q_k 0}; 0, \mathbf{P}_{y,k}^{q_k} \right) \tag{23}$$

After that, the posterior probability of mode $q_k$ and the mode at time $k$ can be derived as follows:

$$\begin{cases} \alpha_{k,q_k}^{+} = \dfrac{p(\mathbf{y}_k|q_k, \mathbf{Y}_{k-1}) p(q_k|\mathbf{Y}_{k-1})}{\sum_{q_k=1}^{n_m} p(\mathbf{y}_k|q_k, \mathbf{Y}_{k-1}) p(q_k|\mathbf{Y}_{k-1})} = \dfrac{\Lambda_{k,q_k} \alpha_{k,q_k}^{-}}{\sum_{q_k=1}^{n_n} \Lambda_{k,q_k} \alpha_{k,q_k}^{-}} \\ q_k = \arg\max_{q_k} \alpha_{k,q_k}^{+} \end{cases} \tag{24}$$

Thus, the posterior probability of continuous state and its covariance can be obtained as follows:

$$\begin{cases} \hat{\mathbf{x}}_k^{+} = \sum_{j=1}^{n_n} \alpha_{k,q_k}^{+} \hat{\mathbf{x}}_k^{q_k+} \\ \mathbf{P}_k = \sum_{q_k=1}^{n_m} \alpha_{k,q_k}^{+} \left( \left( \hat{\mathbf{x}}_k^{q_k+} - \hat{\mathbf{x}}_k^{+} \right) \left( \hat{\mathbf{x}}_k^{q_k+} - \hat{\mathbf{x}}_k^{+} \right)^T + \mathbf{P}_k^{q_k} \right) \end{cases} \tag{25}$$

### *2.3. Track Projection*

Taking the flight of an aircraft from the initial approach fix (IAF) to the final approach fix (FAF) as an example, we define the aircraft as having a heading-hold (HH) mode and a turning (TN) mode in terms of lateral, and ot has constant height (CH) mode and descent (DT) mode terms longitudinally. Thus, there are four modes defined in this study, containing $m_1 = (HH, CH)$, $m_2 = (TN, CH)$, $m_3 = (HH, DT)$, and $m_4 = (TN, DT)$. The set of modes can be described as $\mathbf{M} = \{m_1, m_2, m_3, m_4\}$.

For simplification, the spherical terrestrial reference was used to calculate the position in a Cartesian frame instead of an ellipsoidal one. Choosing $\mathbf{x} = (x_n, y_n, z_n, \eta_n)^T$ as the state vector, according to laws of kinematics, we can easily obtain $\left( x_n^k, y_n^k, z_n^k \right)$ by given $\left( x_n^{k-1}, y_n^{k-1}, z_n^{k-1} \right)$

$$\left( x_n^k, y_n^k, z_n^k \right)^T = \left( x_n^{k-1}, y_n^{k-1}, z_n^{k-1} \right)^T + \mathbf{C}\left( \dot{x}_n^{k-1}, \dot{y}_n^{k-1}, \dot{z}_n^{k-1}, \ddot{x}_n^{k-1}, \ddot{y}_n^{k-1}, \ddot{z}_n^{k-1} \right)^T \tag{26}$$

where $\mathbf{C}$ is a matrix that varies with the modes, which will be discussed in Section 3 in detail. It is believed that the projection only changes the azimuth rather than the length of

the arc between two points. Thus, the azimuth $\eta_n^k$ by given $\left(x_n^{k-1}, y_n^{k-1}, z_n^{k-1}\right)$ and $\eta_n^{k-1}$ can be obtained as follows:

$$\begin{cases} \eta_n^k = \eta_n^{k-1} + \Delta\eta_n^{k-1} \\ \Delta\eta_n^{k-1} = \arccos((\cos L_1 - \cos L_2 \cos L_3)/(\sin L_2 \sin L_3)\ ) \end{cases} \tag{27}$$

where the second equation is the cosine law with respect to sides of a spherical triangle [28], while $L_1$, $L_2$, and $L_3$ represent the length of the three sides, which can be calculated as shown in Figure 2. $\Delta\eta_n^{k-1}$ is the angle corresponding to side $L_1$.

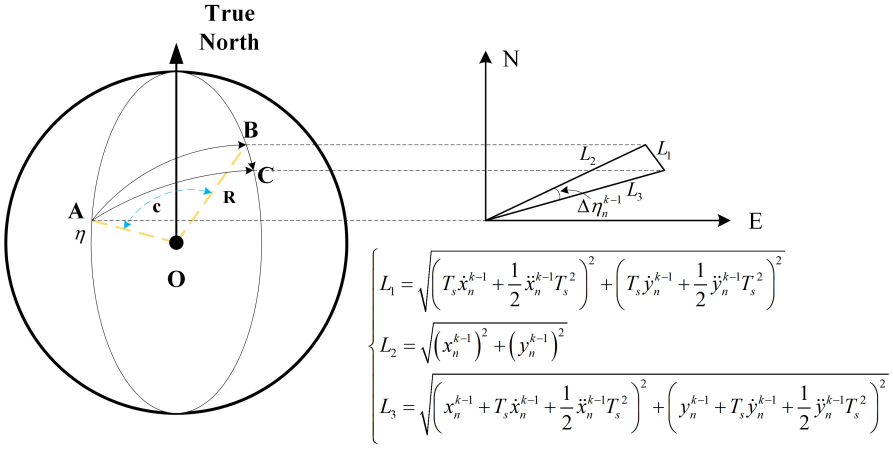


**Figure 2.** Great Circle projection.

Then, the state equation can be built as follows:

$$\mathbf{x}_k = f(\mathbf{x}_{k-1}, \mathbf{u}_{k-1}) + \mathbf{w}_{k-1} \tag{28}$$

where the input matrix $\mathbf{u}_{k-1} = \left(\dot{x}_n^{k-1}, \dot{y}_n^{k-1}, \dot{z}_n^{k-1}, \ddot{x}_n^{k-1}, \ddot{y}_n^{k-1}, \ddot{z}_n^{k-1}\right)^T$.

According to Great Circle projection shown in Figure 2. If the latitudes and longitudes of points A and B are given as $(\phi_A, \lambda_A)$ and $(\phi_B, \lambda_B)$, respectively. The azimuth $\eta$ from A to B can be obtained as follows:

$$\begin{cases} \cos(\angle AOB) = \cos(\frac{\pi}{2} - \phi_B)\cos(\frac{\pi}{2} - \phi_A) + \sin(\frac{\pi}{2} - \phi_B)\sin(\frac{\pi}{2} - \phi_A)\cos(\lambda_B - \lambda_A) \\ \eta = \arcsin(\dfrac{\sin(\frac{\pi}{2} - \phi_B) \times \sin(\lambda_B - \lambda_A)}{\sin(\angle AOB)}) \end{cases} \tag{29}$$

where $\angle AOB$ represents the angle between $OA$ and $OB$. Thus, The Cartesian coordinates of point B relative to point A can be obtained as follows:

$$\begin{cases} x_{BtoA} = L_2\cos(\frac{\pi}{2} - \eta) \\ y_{BtoA} = L_2\sin(\frac{\pi}{2} - \eta) \end{cases} \tag{30}$$

where $L_2$ represents the great circle distance between A and B, which can be calculated as $L_2 = Rc$.

We define the reference point, which is the origin in Cartesian frame, as point A; thus, the coordinate of any point B relative to point A according to Equations (29) and (30) can be described as

$$(x_{BtoA}, y_{BtoA}, \eta)^T = h(\phi_B, \lambda_B) \tag{31}$$

As mentioned above, we can obtain the latitude and longitude of point B by giving the latitude and longitude of point A, the azimuth $\eta$, and the great circle distance $L_2$. In a

short period of time $T_s$, it is believed that the flight distance in a Cartesian frame could be approximately equal to $L_1$. That means that

$$L_1 = \left( \left( T_s \dot{x}_n^{k-1} + \frac{1}{2} \ddot{x}_n^{k-1} {T_s}^2 \right)^2 + \left( T_s \dot{y}_n^{k-1} + \frac{1}{2} \ddot{y}_n^{k-1} {T_s}^2 \right)^2 \right)^{\frac{1}{2}} \tag{32}$$

Consequently, the measurement input can be defined as $\mathbf{y} = (\varsigma, \gamma, h)^T$ while for all modes, the measurement equations are all the same as

$$\mathbf{y}_k = h^{-1}(\mathbf{x}_k) + \mathbf{r}_k \tag{33}$$

## 3. Results and Discussion

### *3.1. Scenario and Parameter Settings*

We take the instrument approach procedure, the base turn-a-specific pattern of reversal procedure, of a certain aircraft on a certain runway with elevation 3567.5 m and magnetic variation 0.3° W as an example. As shown in Figure 3, during the approach, the aircraft would first hold the bearing 107° from the IAF at 7200 m and descend by 1400 m, and then turn to intercept the inbound track at 274° while descending by 150 m. Finally, it descends to 5350 m and then holds the altitude with the constant bearing until the FAF.

For the leg from point IAF to point WPT1, the aircraft descends at a constant speed. After descending with variant speed of the three-axis NED frame for the leg from WPT1 to WPT2, it then descends at an even speed until the point at nearly 5350 m, where it finally keeps a level flight until the FAF. Thus, we obtain the matrix **C** of different modes in Equation (26).

$$\begin{cases} \mathbf{C}_1 = \begin{bmatrix} T_s & 0 & 0 & 0 & 0 & 0 \\ 0 & T_s & 0 & 0 & 0 & 0 \\ 0 & 0 & 0 & 0 & 0 & 0 \end{bmatrix} \; for \; m_1 \\ \varnothing \; for \; m_2 \\ \mathbf{C}_3 = \begin{bmatrix} T_s & 0 & 0 & 0 & 0 & 0 \\ 0 & T_s & 0 & 0 & 0 & 0 \\ 0 & 0 & T_s & 0 & 0 & 0 \end{bmatrix} \; for \; m_3 \\ \mathbf{C}_4 = \begin{bmatrix} T_s & 0 & 0 & {T_s}^2/2 & 0 & 0 \\ 0 & T_s & 0 & 0 & {T_s}^2/2 & 0 \\ 0 & 0 & T_s & 0 & 0 & {T_s}^2/2 \end{bmatrix} \; for \; m_4 \end{cases} \tag{34}$$

where $T_s = 0.1$ s.

We collect data of the altitude $H$ and azimuth $\eta$ at points WPT1, WPT2, and the point where the aircraft has just been performing a level flight, that is, where the mode transition occurs. It is assumed that these data are independent of each other and follow a normal distribution. Statistical analysis is conducted on these data separately to obtain the means $\mu_H$ and $\mu_\eta$, as well as the standard deviations $\sigma_H$ and $\sigma_\eta$. The results are shown in Table 1 in the International System of Units (SI).

**Table 1.** Means and variances of parameters.

| Parameters | WPT1 | | WPT2 | | Level Flight | |
|---|---|---|---|---|---|---|
| | $\mu_H/\mu_\eta$ | $\sigma_H/\sigma_\eta$ | $\mu_H/\mu_\eta$ | $\sigma_H/\sigma_\eta$ | $\mu_H$ | $\sigma_H$ |
| $H(m)$ | 2241.767 | 3.046 | 2086.072 | 2.536 | 1786.758 | 1.653 |
| $\eta(\circ)$ | 108.127 | 1.862 | 274.845 | 1.387 | - | - |

According to the approach procedure, the series of modes is $m_3 \rightarrow m_4 \rightarrow m_3 \rightarrow m_1$, so the probability of mode transition is built as shown in Table 1 for simplification. It

could indeed be simplified like this with only the path from IAF to FAF considered. The probability of the mode transition $\gamma^{q_{k-1}q_k}$ is determined by $a_{q_{k-1}q_k}$, $b_{q_{k-1}q_k}$, $\mathbf{L}_{q_{k-1}q_k}$, $\boldsymbol{\mu}_{q_{k-1}q_k}$, $\boldsymbol{\Sigma}_{k-1}^{q_{k-1}q_k}$, $\hat{\mathbf{x}}_{k-1}^{q_{k-1}}$ and $\mathbf{P}_{k-1}^{q_{k-1}}$. Meanwhile, $\hat{\mathbf{x}}_{k-1}^{q_{k-1}}$ and $\mathbf{P}_{k-1}^{q_{k-1}}$ can be obtained from the results by ASR-UPF, and here, $a_{q_{k-1}q_k} = 0$ and $b_{q_{k-1}q_k} = 1$ were used because of their designability [15]. The variable $\boldsymbol{\mu}_{q_{k-1}q_k}$ and its variance $\boldsymbol{\Sigma}_{k-1}^{q_{k-1}q_k}$ are obtained from Table 1.

We only consider the mode transitions in Table 2. For the transition from $m_3$ to $m_4$, the azimuth $\eta$ and altitude $H$ would decrease, and we define $\mathbf{L}_{34} = \begin{bmatrix} 0 & 0 & 1 & 0 \\ 0 & 0 & 0 & -1 \end{bmatrix}$, $\boldsymbol{\mu}_{34} = (-2239.767, -108.127)^T$ and $\boldsymbol{\Sigma}^{34} = \begin{bmatrix} 3.046^2 & 0 \\ 0 & 1.862^2 \end{bmatrix}$. Thus, $\mathbf{L}_{34}\hat{\mathbf{x}}_{k-1,\cdot|i} - \boldsymbol{\mu}_{34} \geq \mathbf{0}$ when the mode transition happens. For the same mode transition from $m_4$ to $m_3$, we define $\mathbf{L}_{43} = \begin{bmatrix} 0 & 0 & 1 & 0 \\ 0 & 0 & 0 & -1 \end{bmatrix}$, $\boldsymbol{\mu}_{43} = (-2084.072, -274.845)^T$ and $\boldsymbol{\Sigma}^{43} = \begin{bmatrix} 2.536^2 & 0 \\ 0 & 1.387^2 \end{bmatrix}$. For the transition from $m_3$ to $m_1$, it is sufficient to consider the altitude only with $\mathbf{L}_{31} = \begin{bmatrix} 0 & 0 & 1 & 0 \end{bmatrix}$, $\boldsymbol{\mu}_{31} = (-1783.758)$ and $\boldsymbol{\Sigma}^{31} = \begin{bmatrix} 1.653^2 \end{bmatrix}$.

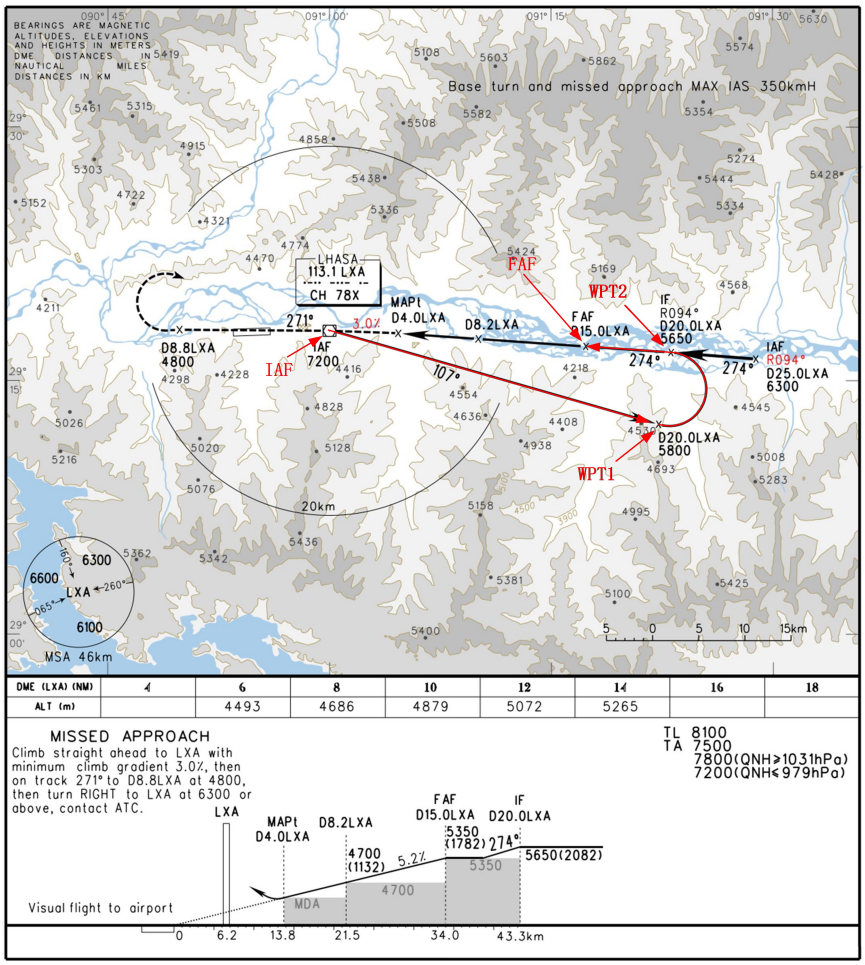


**Figure 3.** Base turn chart.

**Table 2.** The probabilities of mode transition.

| Modes | $m_1$ | $m_2$ | $m_3$ | $m_4$ |
|---|---|---|---|---|
| $m_1$ | 1 | 0 | 0 | 0 |
| $m_2$ | 0 | 0 | 0 | 0 |
| $m_3$ | $\gamma^{31}$ | 0 | $1-\gamma^{34}-\gamma^{31}$ | $\gamma^{34}$ |
| $m_4$ | 0 | 0 | $\gamma^{43}$ | $1-\gamma^{43}$ |

### *3.2. Estimation Results*

The following tests were conducted to verify the performance of the nonlinear stochastic hybrid estimation of the synthetic filtering system. It is undesirable to test the algorithm by comparing the estimation results with recorded flight data directly because the measurements from in-flight data are not accurate in terms of noise and some unexpected disturbances and cannot be regarded as the true value, and there is even a lack of records fir some data. Instead, a flight dynamics model (FDM) of B737-800 with motion models, aerodynamic models, engine models, and control system models, etc., was used to provide standard flight variables for comparison.

Based on the approach procedure mentioned above, the estimation results of ASR-UPF with 100, 300 and 500 particles and the SR-UKF were compared to each other to illustrate the estimation accuracy. The two noise covariance matrices in the FDM can be set freely because of the robustness in the adaptive scheme [29]. While or fast convergence, the proper values were set with $\mathbf{Q}_0 = diag(1, 1, 1, 0.005)$ and $\mathbf{R}_0 = diag(0.005, 0.005, 1)$. The forgetting factor in ASR-UPF was set by $b = 0.9$. Figure 4 shows the estimation error of the position and azimuth by SR-UKF (green line) and the ASR-UPF with 100 (black line), 300 (cyan line), and 500 particles (red line). Both estimation errors were almost the same initially. However, the estimation error of ASR-UPF started convergence at about 3.9 s, 3.0 s, and 2.8 s corresponding to ASR-UPF with 100, 300, and 500 particles, respectively, while the error of the SR-UKS starts convergence at about 6.8s and subsequently ramps up in the filtering process. In addition, the $x_n$, $y_n$, $z_n$ (or $H$) and $\eta$ estimation errors of both algorithms increased significantly at about 399 s and 560 s because there is a delay in mode transition estimation. And the estimation error of $z_n$ by both algorithms increased at about 628 s due to the mode transition from $m_3$ to $m_1$ with a deceleration descent process. In addition, the estimation errors of ASR-UPF with 300 and 500 particles are close.

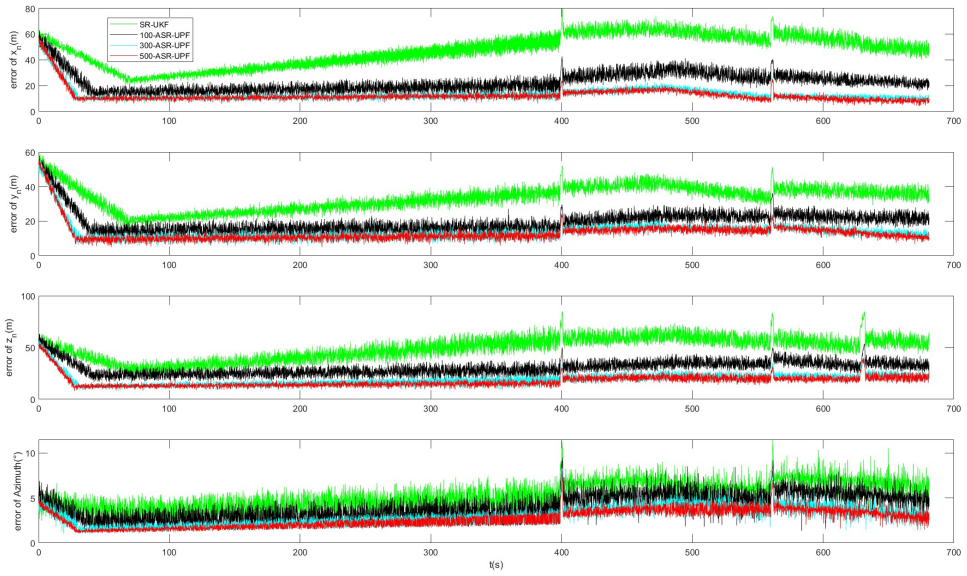


**Figure 4.** Error comparison of position and azimuth accuracy.

The comparison results of mode estimation with the various algorithms are shown in Figures 5–7. Obviously, in Figure 5, there is a bit of delay in mode transitions by both algorithms, while the mode probability variation of ASR-UPF in Figure 6 is more stable than that of SR-UKF in Figure 7, which oscillates slightly. Since the performance of ASR-UPF with 300 and 500 particles is close, we just consider ASR-UPF with 300 particles here. The results of ASR-UPF display a better performance in mode estimation regardless of the number of particles and show more accurate mode estimation and more stable mode transitions as well. We also conducted another 50 simulation experiments, and the average number of mode transition error and the root mean square error (RMSE) of the position

and azimuth for the respective algorithm are given in Table 3. This shows that the RMSE of ASR-UPF is much smaller than that of SR-UKF, as well as the mode transition error, while the RMSEs by ASR-UPF with 300 particles and 500 particles are close.

**Table 3.** RMSE of 50 simulations by SR-UKF and ASRUPF.

| Algorithm | RMSE | | | |
|---|---|---|---|---|
| | $x_n$ (m) | $y_n$ (m) | $z_n$ (m) | $\eta$ (°) |
| SR-UKF | 43.586 | 29.594 | 63.860 | 4.862 |
| ASR-UPF with 100 particles | 20.658 | 21.395 | 25.674 | 4.206 |
| ASR-UPF with 300 particles | 14.377 | 12.593 | 20.805 | 3.551 |
| ASR-UPF with 500 particles | 14.476 | 12.203 | 19.231 | 3.704 |

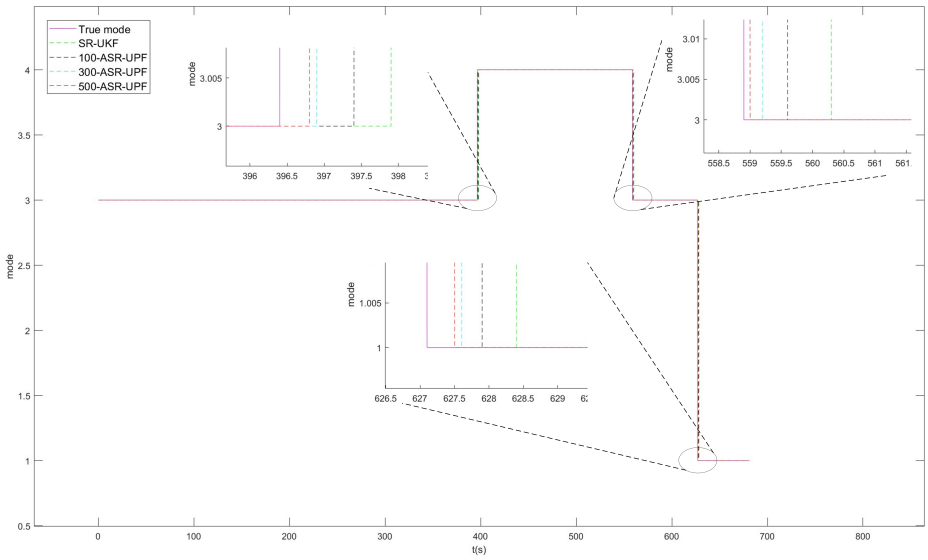


**Figure 5.** Comparison of the accuracy of mode transitions.

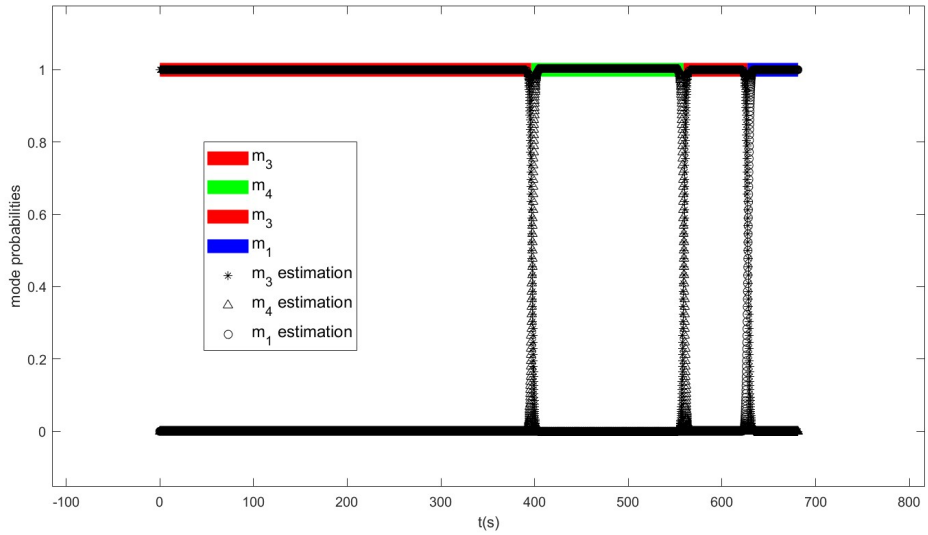


**Figure 6.** Mode probability estimation by ASR-UPF with 300 particles.

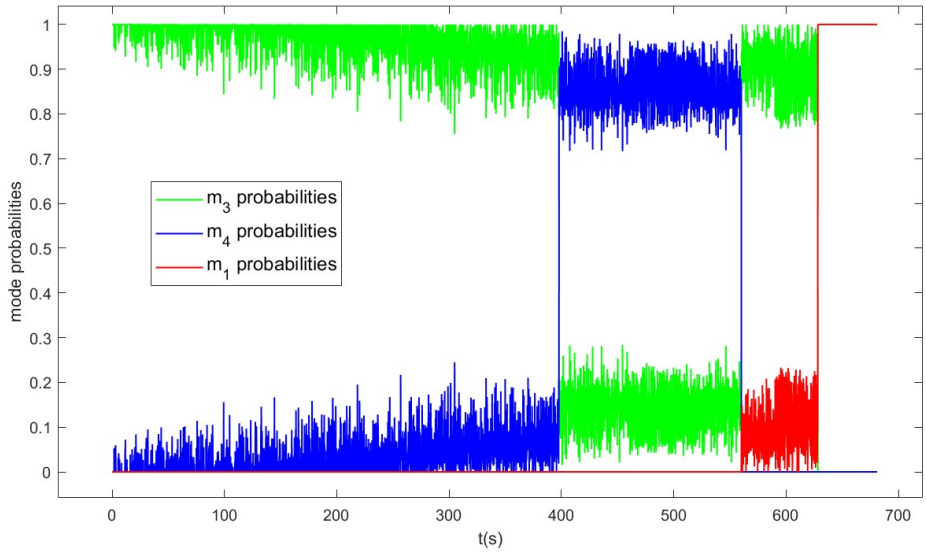


**Figure 7.** Mode probability estimation by SR-UKF.

### *3.3. Results of ASR-UPF Based on Real Flight Data*

The synthetic filtering system and ASR-UPF were applied to real flight-data-based nonlinear hybrid estimation. There is a problem to be addressed before the estimation based on real flight data. The system update and measurement update may not be performed simultaneously because the sampling rates of related variables are probably different. Under normal circumstances, the system update and measurement update are carried out simultaneously. When there are no measurements, only the system update is executed by unequal interval filtering [30].

Still taking the approach procedure in Figure 3 as an example, the measurements and estimated results according to the flight data are shown in Figure 8. Results indicate that the trend of the estimated height approximates that of the recorded flight data, though there were deviations between the estimated $z_n$ and the recorded values. The horizontal coordinates in the NED frame and azimuth without magnetic variation of the aircraft relative to VOR, not the measured in-flight data, could be estimated by the synthetic filtering system as shown in Figure 8a,b. According to the test, the convergence of ASR-UPF was slower than the simulation results by approximately 11s, but the subsequent error slightly increased, as shown in Figure 8c.

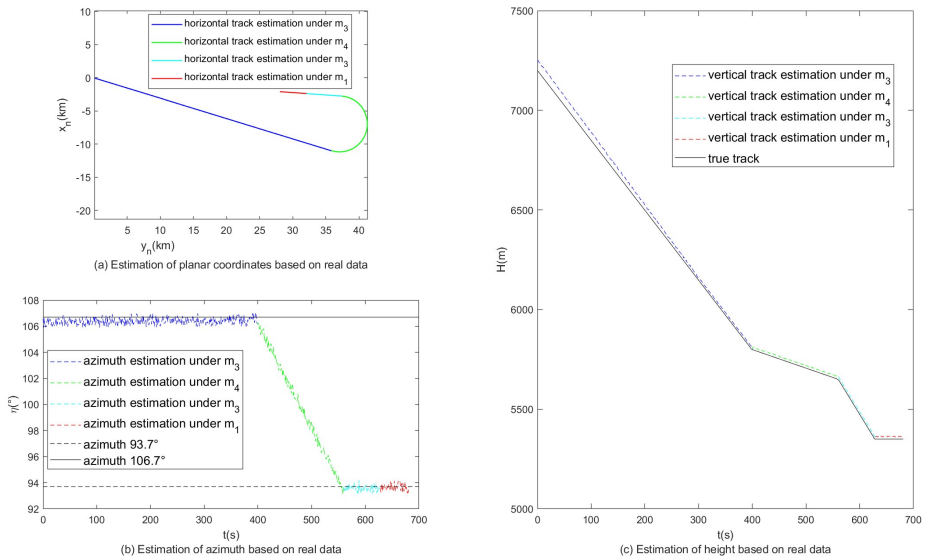


**Figure 8.** Estimation with respect to real flight data.

## 4. Discussion

To improve the estimation accuracy, this study provides a hybrid estimation of positioning, in a Cartesian frame, of an aircraft based on flight data with different modes or patterns of the aircraft's continuous motion considered. The mode estimation, characterized by state-dependent transitions, ensures the accurate modeling for the continuous system. Meanwhile, the ASR-UPF introducing the SR-UKF to generate the importance sampling distribution fully utilizes measurements and guarantees the convergence while maintaining the computational stability of the filter. Otherwise, the adaptive update by tracking noise for reducing errors caused by modeling and measuring improves the robustness to the stochastic noise and enables aircraft positioning with better accuracy.

Though the proposed algorithm is validated based on real flight data, the estimation accuracy needs to be improved further. Also, the resolution and accuracy of inertial measurements, used as the control variable, depend on different flight-data-acquisition systems. Therefore, the estimation performance based on the inertial measurements of a specific aircraft needs to be explored in depth. In addition, this study only considered the transition between two modes because of the specific approach procedure, although there were four modes that were artificially defined. More complex circumstances with transitions between more than two modes, like changing the flight schedule due to some unexpected events (such as encountering windshear), should be studied in depth.

## 5. Conclusions

This study proposes a nonlinear stochastic hybrid filtering system integrated with the Great Circle projection and adaptive square root unscented particle filter. Compared with other research, more accurate state and measurement equations are provided through the projection from longitudes and latitudes in the WGS-84 frame to coordinates in the NED frame, although existing errors are caused by using a spherical reference system for coordinate conversion. The ASR-UPF is recommended for use within position and azimuth estimation applications based on flight data. Since the inertial measurements are insusceptible to external disturbance, without loss of generality, the proposed algorithm could be applied for the refinement of other variables that are not recorded in flight data as well. As a data-driven method, it is a suitable candidate for discrete and continuous state estimation of civil aviation aircraft in specific scenarios.

**Author Contributions:** Data curation, K.Q.; Formal analysis, K.Q. and J.L.; Funding acquisition, K.Q.; Investigation, Z.G. and Y.Z.; Methodology, Y.Z. and Z.G.; Project administration, Z.G.; Resources, K.Q.; Software, Y.Z.; Supervision, Z.G.; Validation, Y.Z. and J.L.; Visualization, Y.Z. and J.L.; Writing—original draft, Y.Z. and Z.G.; Writing—review and editing, Y.Z. and Z.G. All authors have read and agreed to the published version of the manuscript.

**Funding:** This study was funded by the National Natural Science Foundation of China (U2333202, 52272351), the Aeronautical Science Foundation of China (2022Z066052002), and the Civil Aviation Administration of China (ASSA2023/22).

**Data Availability Statement:** Restrictions apply to the availability of these data. Data were obtained from Shandong Airline and are available from Kai, Qi with the permission of Shandong Airline.

**Acknowledgments:** The authors acknowledge the flight data provided by Shandong Airlines.

**Conflicts of Interest:** The authors declare no conflicts of interest.

## Abbreviations

The following abbreviations are used in this manuscript:

| | |
|---|---|
| PBN | Performance Based Navigation |
| GPS | Global Positioning System |
| NED | North, East, and Down |
| WGS-84 | World Geodetic System 1984 |
| ASR-UPF | Adaptive square-root unscented particle filter |

| | |
|---|---|
| SR-UKF | Square-root unscented Kalman filter |
| MLDM | Mixed logical dynamic model |
| GFHMM | Generalized fuzzy hidden Markov model |
| IMM | Interacting multiple model |
| SDTHE | State-dependent transition hybrid estimation |
| EKF | Extended Kalman filter |
| UKF | Unscented Kalman filter |
| CKF | Cubature Kalman filter |

## Appendix A

### *Appendix A.1*

The fundamental square root unscented Kalman filtering algorithm, from which the ASR-UPF is derived, is described as follows. The SR-UKF is initialized according to Equation (19).

At each time step $t_{k-1}$, a group of $2n+1$ sigma points are selected as

$$\begin{cases} \boldsymbol{\mathcal{O}}_{k-1}^{q_k 0(0)+,n_p} = \hat{\mathbf{x}}_{k-1}^{q_k 0,n_p} \\ \boldsymbol{\mathcal{O}}_{k-1}^{q_k 0(row)+,n_p} = \hat{\mathbf{x}}_{k-1}^{q_k 0,n_p} + \sqrt{n+\lambda}\mathbf{S}_{k-1}^{q_k 0,n_p,row}, row = 1,...,n \\ \boldsymbol{\mathcal{O}}_{k-1}^{q_k 0(n+row)+,n_p} = \hat{\mathbf{x}}_{k-1}^{q_k 0,n_p} - \sqrt{n+\lambda}\mathbf{S}_{k-1}^{q_k 0,n_p,row}, row = 1,...,n \end{cases} \tag{A1}$$

where $\mathbf{S}_{k-1}^{q_k 0,n_p,row}$ represents the $row_{th}$-column of square root matrix $\mathbf{S}_{k-1}^{q_k 0,n_p}$. A group of weights related to each sigma point is set by

$$\begin{cases} W_0^{q_k 0,n_p(m)} = \dfrac{\lambda}{n+\lambda} \\ W_0^{q_k 0,n_p(c)} = \dfrac{\lambda}{n+\lambda} + 1 - p_g^2 + p_h \\ W_{row}^{q_k 0,n_p(m)} = W_{row}^{q_k 0,n_p(c)} = \dfrac{1}{2(n+\lambda)} row = 1,2,\ldots\ldots,2n \end{cases} \tag{A2}$$

where $W_{row}^{q_k 0,n_p(m)}$ and $W_{row}^{q_k 0,n_p(c)}$ represent the weights related to the mean and covariance of $\hat{\mathbf{x}}$ each. The constant $p_a \in [0.0001, 1]$ determines the spread of the sigma points around $\hat{\mathbf{x}}$. The constant $p_b$, used to incorporate prior knowledge of the distribution of $\hat{\mathbf{x}}$, is set as $p_b = 2$ for Gaussian distribution. $\lambda = n(p_a^2 - 1)$ is the scaling parameter. The update process of SR-UKF is described by

$$\begin{cases} \hat{\mathbf{x}}_k^{q_k 0,n_p(row)-} = f(\boldsymbol{\mathcal{O}}_{k-1}^{q_k 0(row),n_p+})\ \hat{\mathbf{x}}_k^{q_k 0,n_p-} = \sum_{row=0}^{2n} W_{row}^{q_k 0,n_p(m)} \hat{\mathbf{x}}_k^{q_k 0,n_p(row)-} \\ \mathbf{S}_k^{q_k 0,n_p-} = qr\left\{ \left[ \sum_{row=0}^{2n} \sqrt{W_{row}^{q_k 0,n_p(c)}} (\hat{\mathbf{x}}_k^{q_k 0,n_p(row)-} - \hat{\mathbf{x}}_k^{q_k 0,n_p-})^T, \sqrt{\mathbf{Q}_{k-1}^{q_{k-1},n_p}} \right]^T \right\} \\ \mathbf{S}_k^{q_k 0,n_p-} = cholupdate(\mathbf{S}_k^{q_k 0,n_p-}, \sqrt{\left|W_0^{q_k 0,n_p(c)}\right|} (\hat{\mathbf{x}}_k^{q_k 0,n_p(row)-} - \hat{\mathbf{x}}_k^{q_k 0,n_p-})^T, ' sgn(W_0^{q_k 0,n_p(c)})') \end{cases} \tag{A3}$$

where *cholupdate* represents the Cholesky factor update and sgn represents the sign of $W_0^{q_k 0,n_p(c)}$. As the square root of the error covariance matrix, $\mathbf{S}_k^{q_k 0,n_p-}$ is computed by QR decomposition and Cholesky factor update successively. Note that if $\mathbf{S}$ is the original Cholesky factor of $\mathbf{P} = \mathbf{A}\mathbf{A}^T$, then the Cholesky factor of the rank-1 update (or downdate) $\mathbf{P} \pm \mathbf{m}\mathbf{m}^T$ is denoted as $\mathbf{S} = cholupdate(\mathbf{S}, \mathbf{m}, ' \pm ')$. If $\mathbf{m}$ is a matrix with M columns, the result is M consecutive updates of the Cholesky factor by using the M columns of $\mathbf{m}$.

The next step is to carry out the measurement update. Another group of $2n+1$ sigma points is selected according to the priori estimation $\hat{\mathbf{x}}_k^{q_k 0,n_p-}$ as

$$\begin{cases} \boldsymbol{\mathcal{O}}_k^{q_k 0,n_p(0)-} = \hat{\mathbf{x}}_k^{q_k 0,n_p-} \\ \boldsymbol{\mathcal{O}}_k^{q_k 0,n_p(row)-} = \hat{\mathbf{x}}_k^{q_k 0,n_p-} + \sqrt{n+\lambda}\mathbf{S}_k^{q_k 0,n_p(row)-}, row = 1,\ldots,n \\ \boldsymbol{\mathcal{O}}_k^{q_k 0,n_p(n+row)-} = \hat{\mathbf{x}}_k^{q_k 0,n_p-} - \sqrt{n+\lambda}\mathbf{S}_k^{q_k 0,n_p(row)-}, row = 1,\ldots,n \end{cases} \tag{A4}$$

The priori estimation of measurements is

$$\begin{cases} \hat{\mathbf{y}}_k^{q_k 0,n_p(row)-} = h(\boldsymbol{\mathcal{O}}_k^{q_k 0,n_p(row)-}) \\ \hat{\mathbf{y}}_k^{q_k 0,n_p-} = \sum_{row=0}^{2n} W_{row}^{q_k 0,n_p(m)} \hat{\mathbf{y}}_k^{q_k 0,n_p(row)-} \end{cases} \tag{A5}$$

The measurement update is performed as

$$\begin{cases} \mathbf{S}_{y,k}^{q_k,n_p} = qr\left\{ \left[ \sum_{row=0}^{2n} \sqrt{W_{row}^{q_k 0,n_p(c)}} \left( \hat{\mathbf{y}}_k^{q_k 0,n_p(row)-} - \hat{\mathbf{y}}_k^{q_k 0,n_p-} \right) \quad \sqrt{\mathbf{R}_k^{q_k,n_p}} \right] \right\} \\ \mathbf{S}_{y,k}^{q_k,n_p} = cholupdate(\mathbf{S}_{y,k}^{q_k,n_p}, \sqrt{\left|\mathbf{W}_0^{q_k 0,n_p(c)}\right|}(\hat{\mathbf{y}}_k^{q_k 0,n_p(0)-} - \hat{\mathbf{y}}_k^{q_k 0,n_p-}), ' sgn(W_0^{q_k 0,n_p(c)})') \\ \mathbf{P}_{xy,k}^{q_k,n_p} = \sum_{row=0}^{2n} W_{row}^{q_k 0,n_p(c)} (\hat{\mathbf{x}}_k^{q_k 0,n_p(row)-} - \hat{\mathbf{x}}_k^{q_k 0,n_p-})(\hat{\mathbf{y}}_k^{q_k 0,n_p(row)-} - \hat{\mathbf{y}}_k^{q_k 0,n_p-})^T \\ \mathbf{K}_k^{q_k,n_p} = \mathbf{P}_{xy,k}^{q_k,n_p} \mathbf{S}_{y,k}^{q_k,n_p} \left( (\mathbf{S}_{y,k}^{q_k,n_p})^T \right)^{-1} \\ \hat{\mathbf{x}}_k^{q_k 0,n_p+} = \hat{\mathbf{x}}_k^{q_k 0,n_p-} + \mathbf{K}_k^{q_k,n_p} (\mathbf{y}_k - \hat{\mathbf{y}}_k^{q_k 0,n_p-}) \\ \mathbf{U}_k^{q_k,n_p} = \mathbf{K}_k^{q_k,n_p} \mathbf{S}_{y,k}^{q_k,n_p} \\ \mathbf{S}_k^{q_k 0,n_p} = cholupdate(\mathbf{S}_k^{q_k 0,n_p-}, \mathbf{U}_k^{q_k,n_p}, ' -') \end{cases} \tag{A6}$$

where the square root of the measurement noise covariance matrix $\mathbf{S}_{y,k}^{q_k,n_p}$ is obtained by QR decomposition and Cholesky factor of rank-1 as well. $\mathbf{P}_{xy,k}^{q_k,n_p}$ is the cross-covariance between $\hat{\mathbf{x}}_k^{q_k 0,n_p-}$ and $\hat{\mathbf{y}}_k^{q_k 0,n_p-}$. $\mathbf{K}_k^{q_k,n_p}$ is the filtering gain. With the above operations, the square root of error covariance matrix $\mathbf{S}_k^{q_k 0,n_p}$ is obtained.

## References


1. ICAO. *ICAO 9613 Performance-Based Navigation (PBN) Manual*; ICAO: Montreal, QC, Canada, 2013. Available online: https://standards.globalspec.com/std/1687641/icao-9613 (accessed on 16 May 2024).
2. Pretto, M.; Giannattasio, P.; De Gennaro, M. Mixed analysis-synthesis approach for estimating airport noise from civil air traffic. *Transp. Res. Part D Transp. Environ.* **2022**, *106*, 103248. [CrossRef]
3. Nandiganahalli, J.S.; Lee, S.; Hwang, I. Formal Verification for Mode Confusion in the Flight Deck Using Intent-Based Abstraction. *J. Aerosp. Inf. Syst.* **2016**, *13*, 343–356. [CrossRef]
4. Menci, M.; Papi, M.; Smarrazzo, F. Existence of solutions for coupled hybrid systems of differential equations for mi-croscopic dynamics and local concentrations. *Commun. Pure Appl. Anal.* **2023**, *22*, 2146–2168. [CrossRef]
5. Degani, A.; Shafto, M.; Kirlik, A. Modes in Human-Machine Systems: Constructs, representation and classification. *Int. J. Aviat. Psychol.* **1999**, *9*, 125–138. [CrossRef]
6. Sirmatel, I.I.; Geroliminis, N. Mixed logical dynamical modeling and hybrid model predictive control of public transport operations. *Transp. Res. Part B Methodol.* **2018**, *114*, 325–345. [CrossRef]
7. Pataro, I.M.L.; Gil, J.D.; da Americano C.M.V.; Guzmán, J.L.; Berenguel, M. A nonlinear control approach for hybrid solar thermal plants based on operational conditions. *Renew. Energy* **2022**, *183*, 114–129. [CrossRef]
8. Lyu, H.; Nandiganahalli J.S.; Hwang, I. Human Automation Interaction Issue Detection Using a Generalized Fuzzy Hidden Markov Model. In Proceedings of the AIAA Information Systems-AIAA Infotech at Aerospace, Grapevine, TX, USA, 9–13 January 2017. [CrossRef]
9. Lyu, H.; Nandiganahalli J.S.; Hwang, I. Automation intent inference using the GFHMM for flight deck mode confusion detection. *J. Aerosp. Inf. Syst.* **2018**, *15*, 172–177. [CrossRef]
10. Arroyo, C.A.; Asensio, V.M. Adaptive IMM-UKF for Airborne Tracking. *Aerospace* **2023**, *10*, 698. [CrossRef]

11. Yin, J.; Yang, Z.; Luo, Y. Adaptive tracking method for non-cooperative continuously thrusting spacecraft. *Aerospace* **2021**, *8*, 244. [CrossRef]
12. Ebrahimi, M.; Ardeshiri, Mahdi.; Alaie K.S. Bearing-only 2D maneuvering target tracking using smart interacting multiple model filter. *Digit. Signal Process.* **2022**, *126*, 103497. [CrossRef]
13. Xu, W.; Xiao, J.; Xu, D.. Wang, H.; Cao, J. An Adaptive IMM Algorithm for a PD Radar with Improved Maneuvering Target Tracking Performance. *Remote Sens.* **2024**, *16*, 1051. [CrossRef]
14. Seah, C.E.; Hwang, I. Stochastic Linear Hybrid Systems: Modeling, Estimation, and Application in Air Traffic Control. *IEEE Trans. Control Syst. Technol.* **2009**, *17*, 563–575. [CrossRef]
15. Lee, S.; Hwang, I.; Leiden, K. Intent Inference-Based Flight-Deck Human-Automation Mode-Confusion Detection. *J. Aerosp. Inf. Syst.* **2015**, *12*, 503–518. [CrossRef]
16. Lee, J.; Hwang, I.; Shim, D.H. UAS surveillance in low-altitude airspace with geofencing: Constrained stochastic linear hybrid systems approach. In Proceedings of the 2018 AIAA Information Systems-AIAA Infotech @ Aerospace, Kissimmee, FL, USA, 8–12 January 2018. [CrossRef]
17. Shan, D.; Wang, D.; He, D.; Zhang, P. Position Sensorless Vector Control System for Lawnmower Permanent Magnet Synchronous Motor Based on Extended Kalman Filter. *Energies* **2024**, *17*, 1230. [CrossRef]
18. Khan, A.B.; Akram, A.S.; Choi, W. State of Charge Estimation of Flooded Lead Acid Battery Using Adaptive Unscented Kalman Filter. *Energies* **2024**, *17*, 1275. [CrossRef]
19. Lv, Y.; Liu, S.; Gao, Y.; Dai, J.; Ren, Z.; Liu, Y. An Ultra-Wideband Indoor Localization Algorithm with Improved Cubature Kalman Filtering Based on Sigmoid Function. *Appl. Sci.* **2024**, *14*, 2239. [CrossRef]
20. Tivay, A.; Hahn, J. A Population-Informed Particle Filter for Robust Physiological Monitoring Using Low-Information Time-Series Measurements. *IEEE Trans. Biomed. Eng.* **2023**, *70*, 2298–2309. [CrossRef] [PubMed]
21. Zare, H.; Weber, T.K.D.; Ingwersen, J.; Nowak, W.; Gayler, S.; Streck, T. Combining Crop Modeling with Remote Sensing Data Using a Particle Filtering Technique to Produce Real-Time Forecasts of Winter Wheat Yields under Uncertain Boundary Conditions. *Remote Sens.* **2024**, *14*, 1360. [CrossRef]
22. Kanthalakshmi, S.; Raghappriya, M. Active fault diagnosis of 2 DoF helicopter using particle filter-based log-likelihood ratio. *Int. J. Control* **2022**, *95*, 3148–3165. [CrossRef]
23. Peng, S.; Zhang, A.; Liu, D.; Cheng, M.; Kan, J.; Pecht, M. State-of-Charge Estimation of Lithium-Ion Batteries Based on Dual-Coefficient Tracking Improved Square-Root Unscented Kalman Filter. *Batteries* **2023**, *9*, 392. [CrossRef]
24. Janjanam, L.; Saha, S.K.; Kar, R.; Mandal, D. Hammerstein-Wiener nonlinear system identification by using honey badger algorithm hybridized Sage-Husa adaptive Kalman filter with real-time applications. *Int. J. Electron. Commun.* **2022**, *151*, 154218. [CrossRef]
25. Seah, C.E.; Hwang, I. State Estimation for Stochastic Linear Hybrid Systems with Continuous-State-Dependent Transitions: An IMM Approach. *IEEE Trans. Aerosp. Electron. Syst.* **2009**, *45*, 376–392. [CrossRef]
26. Fazilova, D. Uzbekistan's coordinate system transformation from CS42 to WGS84 using distortion grid model. *Geod. Geodyn.* **2022**, *13*, 24–30. [CrossRef]
27. Wang, P.; Wang, M.; Yang, Y. Particle Filter with improved MSV Resample for Manoeuvring Target Tracking. In Proceedings of the 2020 Chinese Automation Congress (CAC), Shanghai, China, 6–8 November 2020; pp. 6522–6527. [CrossRef]
28. Petrera, M.; Suris, Y.B. Spherical geometry and integrable systems. *Geom. Dedicata* **2014**, *169*, 93–98. [CrossRef]
29. Gao, Z.; Zhang, Y.; Ochieng, W.Y.; Xiang, Z. Adaptive Air-Data Smoothing Estimation with Customized Wind Model Based on Flight Data. *J. Aerosp. Eng.* **2022**, *35*, 04022054. [CrossRef]
30. Gao, Z.; Wang, H.; Xiang, Z. Flight Data-Based Wind Disturbance and Air Data Estimation. *Atmosphere* **2021**, *12*, 470. [CrossRef]